Arch. Min. Sci. **70** (2025), 3, 423-452

Electronic version (in color) of this paper is available: http://mining.archives.pl

DOI: https://doi.org/10.24425/ams.2025.156293

TONG WANG[1,2*], KE YANG[1,2], YONGPING WU[3],
PANSHI XIE[3], XIAOLOU CHI[1,2]

STABILITY OF MULTI-DIMENSIONAL SYSTEM OF PARALLELOGRAM SUPPORT IN PSEUDO-INCLINED LONGWALL FULLY MECHANIZED MINING FACE OF STEEPLY DIPPING COAL SEAM

The key to safe and efficient mining of pseudo-inclined working face of steeply dipping coal seam is the stability control of 'support-surrounding rock' system. Based on the comprehensive determination of the load characteristics of the support in the working face, the overall stability and internal component load characteristics of the parallelogram hydraulic support under the influence of different factors are analyzed. The results show that: (1) The working resistance of the column gradually decreases with the increase of the angle of seam; the working resistance of the balance jack, the force of the front and back link all increase with the increase of the angle of seam. (2) The working resistance of the column and the working resistance of the balance jack increase, and the inclined and strike components of the constraint force of the hinge point of the top beam-shield beam change greatly. The top beam of the support is affected by the eccentric load, which affects the stability of the support and is prone to falling and sliding. (3) The parallelogram support also reaches the maximum stress at the connection between the column and the top beam, and the stress of the shield beam is relatively small.

Keywords: Stability analysis; steeply dipping coal seam; pseudo-inclined working face; parallelogram support; multi-dimensional and multi-objective system

[1] ANHUI UNIVERSITY OF SCIENCE AND TECHNOLOGY, SCHOOL OF MINING ENGINEERING, HUAINAN, 232001, CHINA
[2] ANHUI UNIVERSITY OF SCIENCE AND TECHNOLOGY,STATE KEY LABORATORY OF MINE RESPONSE AND DISASTER PREVENTION AND CONTROL IN DEEP COAL MINES, HUAINAN, 232001, CHINA
[3] XI'AN UNIVERSITY OF SCIENCE AND TECHNOLOGY, SCHOOL OF ENERGY ENGINEERING, XI'AN 710054, CHINA
[4] XI'AN UNIVERSITY OF SCIENCE AND TECHNOLOGY, KEY LABORATORY OF WESTERN MINE EXPLOITATION AND HAZARD PREVENTION MINISTRY OF EDUCATION, XI'AN 710054, CHINA

* Corresponding author: 670298140@qq.com

1. Introduction

The term “steeply dipping coal seam” denotes a seam characterized by a burial dip angle ranging from 35° to 55° [1]. This coal seam is widely acknowledged as challenging within the global mining industry [2]. Over 50% of steeply dipping coal seams consist of high-quality coking coal, anthracite, and other rare coal varieties. In China’s western regions, such as Sichuan, Xinjiang, and Gansu, over half of the mines predominantly extract steeply dipping coal seams, largely due to the challenging terrain. Prolonged high-intensity mining in eastern China has depleted reserves of easily accessible coal seams, prompting a shift to mining steeply dipping seams with more complex geological conditions [3]. Consequently, the extraction of steeply dipping coal seams constitutes a significant challenge confronting the progression of China’s mining sector. Safe and efficient mining practices represent the pivotal and challenging focal point for advancing mechanized mining capabilities within China’s coal industry, playing a crucial role in driving regional economic and social development.

In recent years, advancements in science and technology have substantially enhanced the mechanized longwall mining capabilities within steeply dipping coal seams under specific conditions. Nonetheless, significant challenges persist in actual production due to the substantial disparities between the support-surrounding rock interaction systems in steeply dipping coal seams and those in horizontal coal seams [4,5]. In contrast to horizontal coal seams, the inclined orientation of steeply dipping coal seams amplifies the gravitational component of support while diminishing the vertical component during mining operations. This alteration diminishes support stability, leading to frequent occurrences of support sliding, collapsing, inter-frame extrusion, and wedging [6,7]. Moreover, the support operates within a non-equilibrium complex stress environment influenced by factors such as roof and floor strata, coal walls, gangue, and adjacent supports [8-10]. Through theoretical analysis, numerical calculations, physical similar material simulation experiments, and field monitoring, numerous scholars have investigated and delved into the migration patterns of surrounding rock and the load characteristics of support structures under various mining methods. These methods include long-wall mining of medium-thick coal seams, long-wall fully-mechanized caving of thick coal seams, and combined mining of coal seam groups. They have examined the coupling mechanism and variation instability mechanism within the ‘support-surrounding rock’ system [11-14], as well as the push-out phenomenon between supports and its cumulative effects [15-17]. Additionally, they have established criteria for support stability assessment and devised methods for calculating the critical working resistance of support stability [18], while proposing technical measures to prevent collapse and sliding of hydraulic support systems [19]. This advancement has catalyzed the ongoing evolution of both the theoretical framework and technological advancements in controlling support stability within steeply dipping coal seam mining operations. The aforementioned research findings contribute to ensuring support stability to some extent. However, these studies are primarily conducted on a two-dimensional plane and lack the capacity to quantitatively describe the mechanical response and behavior of hydraulic supports in a three-dimensional spatial context. Hence, in practical applications of steeply dipping coal seam mining, challenges persist, including inadequate support stability and difficulty in repositioning after instability events, leading to diminished production efficiency and compromised safety standards.

Under the background of this research, some scholars have proposed the pseudo-inclined mining method [20]. The pseudo-inclined mining method effectively decreases the dip angle of the working face, thereby enhancing support stability and mitigating the risk of dynamic

disasters such as coal wall spalling and airborne gangue. Achieving safe and efficient production in long-wall fully mechanized mining faces within steeply dipping coal seams holds immense significance [21]. However, due to the oblique intersection of the pseudo-inclined working face with the tailgate and headgate, when employing a rectangular top beam for support, the support arrangement adopts a stepped configuration, which can lead to tail swing and bottom pushing tendencies during the process. The gap between the front of the top beam of the support and the coal wall facilitates the entry of gangue into the working space, posing operational challenges. Additionally, the exposed end of the support is susceptible to impacts from gangue in the gob, compromising the support's stability. In response to these challenges, Xi'an University of Science and Technology collaborated with Liuzhi Industrial and Mining Group to conduct joint research and develop an innovative special-shaped support system. The top beam of the special-shaped support features a parallelogram shape, specifically designed to seamlessly interface with the coal wall of the large-angle pseudo-inclined fully mechanized mining face.

Building upon this concept, the paper focuses on the engineering context of the 3132 pseudo-inclined long-wall fully mechanized mining face at Lvshuidong Coal Mine. The special-shaped (parallelogram) hydraulic support serves as the primary research subject. Through a combination of theoretical analysis, numerical simulation, and field measurements, a comprehensive three-dimensional spatial mechanics model and numerical representation of the special-shaped support are established. After carefully evaluating the load characteristics of the working face support, the study analyzes the overall stability and internal component load characteristics of the special-shaped hydraulic support. This assessment considers different influencing factors, including seam angle, working face pseudo-inclined angle, gangue force, and the position of the roof load. The study delves into the evolution pattern of stress and deformation within the support group under regional load characteristics. The research findings contribute significantly to enhancing the stability control theory of the multi-dimensional and multi-objective system of support. This enrichment holds substantial importance for optimizing the support structure of pseudo-inclined working faces, implementing field applications of special-shaped supports, and advancing the development of mechanized, safe, and efficient mining in steeply dipping coal seams.

2. Engineering background

The 3132 working face of Lvshuidong Coal Mine is situated in the upper section of the 313 mining area, within the east wing of the Longwangdong anticline, at the +350 meter level. The coal seam angle ranges from 38° to 46°, with an average angle of 43°. The average thickness of the coal seam is 2.5 meters, and its bulk density is 1.44 t/m³. The coal seam comprises semi-dark semi-bright coking coal and coking fat coal, with a relatively stable occurrence. The main roof consists of argillaceous limestone with a rock layer thickness ranging from 3.2 to 8.5 meters and a hardness of $4 \leq f \leq 5$. The immediate roof is composed of calcareous mudstone, with a rock thickness of 2.7 to 3.3 meters and a hardness of $4 \leq f \leq 6$. The immediate floor comprises mudstone and shale, with a rock layer thickness of 2.0 to 3.6 meters and a hardness of $3 \leq f \leq 6$. The lithology of the main floor consists of sandy mudstone, with a rock layer thickness ranging from 1.0 to 3.0 meters and a hardness of $3 \leq f \leq 6$. Fig. 1 illustrates the stratum histogram of the 3132 working face, while TABLE 1 provides the physical and mechanical parameters of the coal and rock mass.

TABLE 1

Physical parameters of coal and rock in 3132 working face

Name	Lithology	Weight Density / kN·m^{-3}	Bulk / MPa	Strength / MPa	Poisson
Main Roof	Argillaceous Limestone	26	1833.6	147.36	0.24
Immediate Roof	Calcareous Mudstone	24.3	1133.3	72.48	0.32
Coal	Coal	17	500	20.16	0.30
Immediate Floor	Mudstone	21.1	1066.7	67.2	0.33
Main Floor	Sandy Mudstone	24	1350	160.8	0.22

In the working face, a pseudo-inclined layout is adopted with a pseudo-inclined angle of 25°. There is a height difference of 77 meters between the roadways, and the advanced headgate of the tailgate is 51 meters. The angle of the working face is reduced from the original seam angle of 45° to 39°. The length of the working face is 120 meters, while the advancing length along the strike is 1022 meters. Using oblique cutting feed for the shearer entails cutting the coal from the tail of the working face to the head in a one-way downward direction. This method offers several advantages, including enhancing the anti-skid capability of the shearer and reducing traction resistance. Additionally, after cutting, the empty cutter returns to the feed location for the next cycle. The hydraulic support is mobilized by the shearer machine, while the scraper conveyor is pushed from the head to the tail after completing the shearer's circulating feed.

To better adapt to the coal wall of the pseudo-inclined working face and align with its direction, providing support for the triangular empty roof in front of the coal wall during the mining process is essential. This proactive measure helps prevent gangue caving and coal wall spalling, ultimately ensuring a safer working environment. Transforming the top beam of the working face support from a rectangle to a parallelogram addresses the issue of the front end of the rectangular top beam support not being parallel to the coal wall. This adjustment ensures better alignment and support along the coal wall, enhancing stability and safety during mining operations.

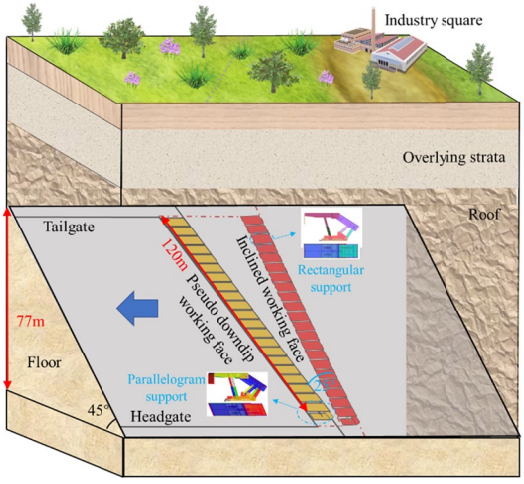

Layer	Histogram	Thickness /m	Description
Main roof		3.2~8.5 / 5.85	The upper is dark gray mudstone, the middle is argillaceous limestone, and the lower is gray black siliceous thin layer limestone.
Immediate roof		2.7~3.3 / 3.0	The upper is dark gray mudstone, and the lower is gray calcareous mudstone. The layer has a sheet structure, and the joints are not well developed, mostly quartz.
False roof		0~0.2 / 0.1	Clay mudstone, thin layer
Coal		2.5	Semi-dark and semi-bright coking coal, coking fat coal, coal seam containing 2 ~ 4 layers of gangue
Immediate floor		2.0~3.6 / 2.8	The strata are mudstone and shale, argillaceous cementation, flaky structure, containing pyrite grains.
Main floor		1.0~3.0 / 2.4	The rock layer is light gray sandy mudstone, the lower is black shale, horizontal bedding, sheet structure.

Fig. 1. Layout of 3132 Working face and comprehensive histogram

3. Stability analysis of parallelogram support in pseudo-inclined working face

In earlier studies, the author's team highlighted that gangue slip filling in pseudo-inclined stopes differs notably from that in true inclined stopes of steeply dipping coal seams [22]. The combined influence of seam angle and pseudo-inclined angle makes caving gangue particularly impactful on support in the middle and lower sections of the working face, increasing the likelihood of reverse slip and torsion pendulum effects. Certainly. In this chapter, a comprehensive examination is undertaken to construct a spatial mechanical model for both rectangular and parallelogram supports. Through meticulous clarification of the roof load type and rigorous analysis of various influential factors such as seam angle, pseudo-inclined angle of the working face, gangue force, and roof load position, a detailed comparison is made regarding their impact on the overall stability of supports and internal component stress. This scholarly endeavor lays a robust theoretical foundation for guiding the nuanced practice of three-dimensional stability control, particularly in the implementation of 'support-surrounding rock' methodologies within the context of this specific stope configuration.

3.1. Construction of spatial mechanical model of rectangular support

Indeed, the stress characteristics of internal components within the support structure provide valuable insights into the dynamic interaction between the support system and the surrounding rock mass. By analyzing these stress patterns, one can discern the intricate mechanisms underlying support instability. This understanding is crucial for optimizing support design and implementation strategies to enhance overall stope stability and safety. To clarify the load characteristics of the support in the pseudo-inclined working face, the top beam and the shield beam of the support are separated. This allows for a detailed stress analysis of each component, providing insight into their individual roles in supporting the surrounding rock mass. Such an analysis is crucial for understanding the behavior of the support system in pseudo-inclined working faces and can guide the design of more effective support structures in similar mining scenarios. The general mathematical equation governing the spatial mechanical model of the two-column support shield support has been formulated [23]. By inputting the pertinent geometric parameters of the support into this equation, one can compute the force exerted on each hinge point of the support accurately. Fig. 2 and Fig. 3 depict the mechanical model of the support shield support, providing visual representations of its structural layout and key components for reference and analysis.

Based on the stress state analysis of the top beam, an equilibrium relationship can be established as follows:

$$R_{1x} + R_{2x} - (P_1 + P_2)\sin\theta_1 - P_E\cos\theta_2 + Q_x + f_x + F_m = 0 \tag{1}$$

$$R_{1z} + R_{2z} + (P_1 + P_2)\cos\theta_1 + P_E\sin\theta_2 - Q_z - G_1\cos\alpha = 0 \tag{2}$$

$$R_{1y} + R_{2y} - F + S_{up} - S_{down} + G_1\sin\alpha - Q_y - f_y = 0 \tag{3}$$

$$(P_1 - P_2)a_1\cos\theta_1 + Q_z a_2 + (R_{1z} - R_{2z})a_3 = 0 \tag{4}$$

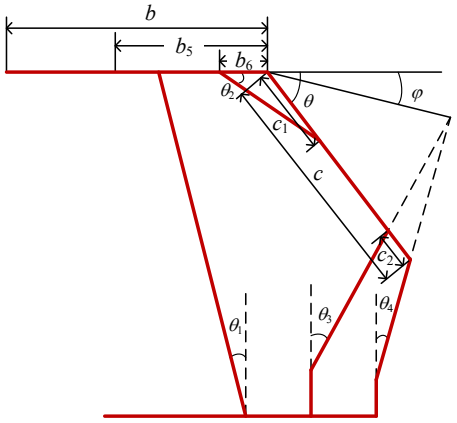

Fig. 2. Supporting-shield support

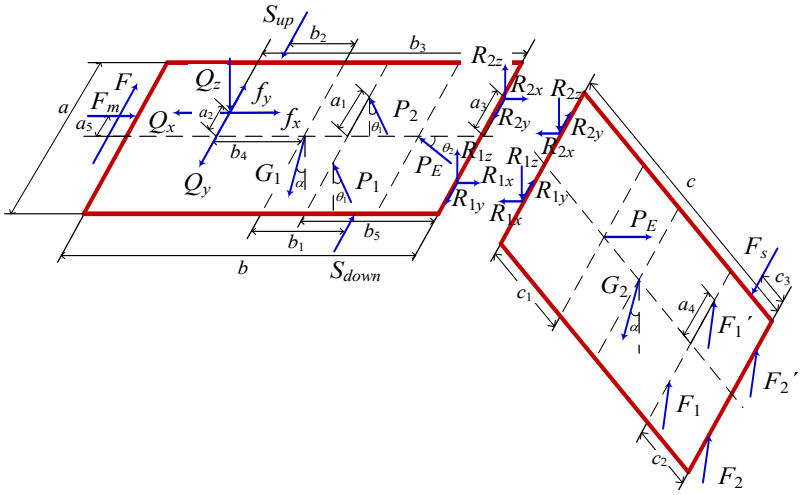

Fig. 3. Mechanical model of rectangular top beam of support

$$(R_{1x}-R_{2x})a_3-(R_{1y}+R_{2y})\frac{b}{2}-Q_xa_2-Q_yb_4-f_xa_2-f_yb_4+S_{up}b_2-$$

$$S_{down}b_1+F\frac{b}{2}+F_ma_5+(P_2-P_1)a_1\sin\theta_1=0 \tag{5}$$

$$Q_zb_3-(P_1+P_2)b_5\cos\theta_1+G_1\frac{b}{2}\cos\alpha-P_Eb_6\sin\theta_2=0 \tag{6}$$

Based on the stress state analysis of the shield beam, the equilibrium relationship can be established as follows:

$$R_{1x}+R_{2x}-P_E\cos\theta_2-(F_1+F_1')\sin\theta_3-(F_2+F_2')\sin\theta_4=0 \tag{7}$$

$$-(R_{1z}+R_{2z})-P_E\sin\theta_2+(F_1+F_1')\cos\theta_3+(F_2+F_2')\cos\theta_4-G_2\cos\alpha=0 \tag{8}$$

$$-(R_{1y}+R_{2y})+F_S+G_2\sin\alpha=0 \tag{9}$$

$$(R_{1x}-R_{2x})a_3\sin\theta+(R_{1z}-R_{2z})a_3\cos\theta+(F_1'-F_1)a_4\cos(\theta-\theta_3)+$$
$$(F_2'-F_2)a_4\cos(\theta-\theta_4)=0 \tag{10}$$

$$(R_{1x}-R_{2x})a_3\cos\theta+(R_{2z}-R_{1z})a_3\sin\theta+(R_{1y}+R_{2y})\frac{c}{2}+$$
$$(F_1-F_1')a_4\sin(\theta-\theta_3)+(F_2-F_2')a_4\sin(\theta-\theta_4)-F_Sc_3=0 \tag{11}$$

$$(F_1+F_1')(c-c_2)\cos(\theta-\theta_3)+(F_2+F_2')c\cos(\theta-\theta_4)+$$
$$P_Ec_1\cos(\theta-\theta_2)-G_2\frac{c}{2}\cos\theta\cos\alpha=0 \tag{12}$$

3.2 Construction of spatial mechanical model of parallelogram support

The equations (1) to (12) represent the mathematical formulation of the spatial mechanical model governing the rectangular top beam shield support. However, it does not incorporate the geometric configuration of the support structure. Building upon its mechanical model, the top beam and shield beam of the support are transformed into a parallelogram shape, where the pseudo-inclined angle is denoted by γ. This modification leads to the establishment of the spatial mechanical model of the parallelogram support, depicted in Fig.4.

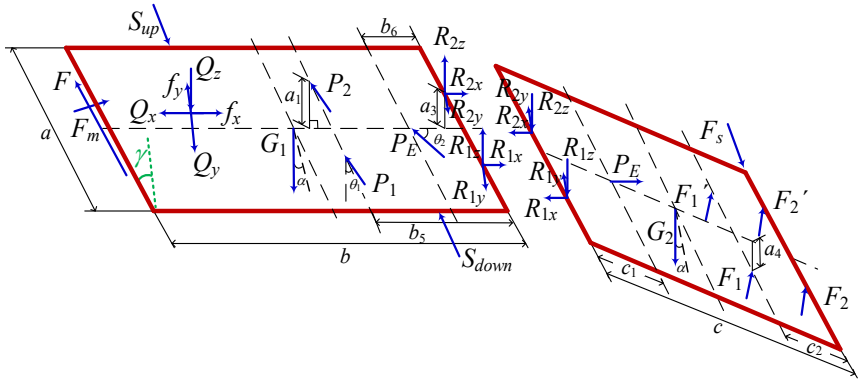

Fig. 4. Mechanical model of parallelogram top beam of support

Based on the stress state analysis of the top beam, the equilibrium relationship can be established as follows:

$$R_{1x}+R_{2x}-(P_1+P_2)\sin\theta_1-P_E\cos\theta_2-Q_x+f_x+F_m\cos\gamma-F\sin\gamma=0 \tag{13}$$

$$R_{1z} + R_{2z} + (P_1 + P_2)\cos\theta_1 + P_E \sin\theta_2 - Q_z - G_1 \cos\alpha = 0 \tag{14}$$

$$R_{1y} + R_{2y} + S_{up} - S_{down} + G_1 \sin\alpha + Q_y - f_y - F_m \sin\gamma - F\cos\gamma = 0 \tag{15}$$

$$(P_1 - P_2)a_1 \cos\theta_1 + Q_z a_2' + (R_{1z} - R_{2z})a_3 = 0 \tag{16}$$

$$(R_{1x} - R_{2x})a_3 - R_{1y}(\frac{b}{2} + a_3 \tan\gamma) - R_{2y}(\frac{b}{2} - a_3 \tan\gamma) + (P_2 - P_1)a_1 \sin\theta_1 -$$
$$f_x a_2' - f_y b_4' + Q_x a_2' + Q_y b_4' + S_{up} b_2' - S_{down} b_1' + F\frac{b}{2}\cos\gamma + F_m a_5' = 0 \tag{17}$$

$$(R_{1z} - R_{2z})a_3 \tan\gamma + Q_z b_3' - P_1(b_5 - a_1 \tan\gamma)\cos\theta_1 + P_2(b_5 + a_1 \tan\gamma)\cos\theta_1 +$$
$$G_1 \frac{b}{2}\cos\alpha - P_E b_6 \sin\theta_2 = 0 \tag{18}$$

Based on the stress state analysis of the shield beam, the equilibrium relationship can be established as follows:

$$R_{1x} + R_{2x} - P_E \cos\theta_2 - (F_1 + F_1')\sin\theta_3 - (F_2 + F_2')\sin\theta_4 = 0 \tag{19}$$

$$-(R_{1z} + R_{2z}) - P_E \sin\theta_2 + (F_1 + F_1')\cos\theta_3 + (F_2 + F_2')\cos\theta_4 - G_2 \cos\alpha = 0 \tag{20}$$

$$-(R_{1y} + R_{2y}) + F_S + G_2 \sin\alpha = 0 \tag{21}$$

$$(R_{1x} - R_{2x})a_3 \sin\theta + (R_{1z} - R_{2z})a_3 \cos\theta + (F_1' - F_1)a_4 \cos(\theta - \theta_3) +$$
$$(F_2' - F_2)a_4 \cos(\theta - \theta_4) = 0 \tag{22}$$

$$(R_{1x} - R_{2x})a_3 \cos\theta + (R_{2z} - R_{1z})a_3 \sin\theta + R_{1y}(\frac{c}{2} - a_3 \tan\gamma) + R_{2y}(\frac{c}{2} + a_3 \tan\gamma) +$$
$$(F_1 - F_1')a_4 \sin(\theta - \theta_3) + (F_2 - F_2')a_4 \sin(\theta - \theta_4) + F_S c_3' = 0 \tag{23}$$

$$[F_1(c - c_2 + a_4 \tan\gamma) + F_1'(c - c_2 - a_4 \tan\gamma)]\cos(\theta - \theta_3) +$$
$$[F_2(c + a_4 \tan\gamma) + F_2'(c - a_4 \tan\gamma)]\cos(\theta - \theta_4) +$$
$$(R_{2z} - R_{1z})a_3 \tan\gamma + P_E c_1 \cos(\theta - \theta_2) - G_2 \frac{c}{2}\cos\theta\cos\alpha = 0 \tag{24}$$

The force system exhibits statically indeterminate characteristics, necessitating the establishment of supplementary equations based on the deformation compatibility condition:

$$\frac{1}{GI_t}[P_1(b_5 - a_1 \tan\gamma) - P_2(b_5 + a_1 \tan\gamma)]a_1 \cos\theta_1 + \frac{1}{GI_t} Q_z a_2 b_3 =$$
$$\frac{1}{G'I_t'}[F_1(c - c_2 + a_4 \tan\gamma) - F_1'(c - c_2 - a_4 \tan\gamma)]a_4 \cos(\theta - \theta_3) +$$
$$\frac{1}{G'I_t'}[F_2(c + a_4 \tan\gamma) - F_2'(c - a_4 \tan\gamma)]a_4 \cos(\theta - \theta_4) \tag{25}$$

In the formula:

α – Angle of seam, °;
γ – Pseudo-inclined angle, °;
P – Column working resistance, kN;
P_E – Working resistance of the Balance jack, the thrust is positive and the tension is negative, kN;
R_{1x}, R_{2x}, R_{1y}, R_{2y}, R_{1z}, R_{2z} – Restraint force of hinge point between roof and shield beam, kN;
F_1, F_1' – Force of the front link, kN;
F_2, F_2' – Force of the back link, kN;
a – Width of support, m;
b – Length of top beam, m;
c – Length of shield beam, m;
θ – The maximum angle between the top beam and the shield beam, °;
θ_1 – Angle between column and vertical direction, °;
θ_2 – The angle between the balance jack and the top beam and the shield beam, °;
θ_3 – Angle between the front link and the vertical direction, °;
θ_4 – Angle between the back link and the vertical direction, °;
G_1, G_2 – Gravity of top beam and shield beam, kN;
Q_x, Q_y, Q_z – X, Y, Z axis Component force of roof load, kN;
f_x,f_y – Friction force between support and roof, kN;
S_{up}, S_{down} – Load between adjacent supports, kN;
F_s – Force of gangue on support, kN;
F_m – Force of coal wall on support, kN;
F – Friction between support and coal wall, kN.

3.3. Analytical expression of mechanics of parallelogram supports

The shield beam plays a crucial role in the support shield hydraulic support system. It's worth noting that the shield beam doesn't provide direct support to the roof. Indeed, the primary role of the shield beam is to enclose the working area, create a barrier between the working space and the goaf, and ensure a safe working environment for the operators. At the same time, as an important force transmission component, the load of the roof and the falling rock can be transmitted to the four-bar linkage mechanism, so that the mechanical state of the 'support-surrounding rock' system remains stable. In the support design, if the angle between the shield beam and the top beam is too small, it can lead to increased load on the shield beam. Additionally, the impact of falling rocks from the roof will also be exerted directly on the shield beam. The excessive load on the shield beam can indeed diminish the support's ability to bear the roof's weight, potentially causing challenges in maneuvering the support system. With the design conditions and experience taken into account, the angle between the top beam and the shield beam is set at 60°. Additionally, the ratio of the shield beam's length to the back link's length is determined to be 2, and the distance between the hinge points of the front and rear connecting rods is set at 0.5 meters. Other parameters are selected as shown in TABLE 2.

TABLE 2

Parameter values of spatial mechanical model of parallelogram support

Parameter	Value
θ_1	10°
θ_2	30°
θ_3	10°
θ_4	5°
a	1.5 m
$2a_1$	1.2 m
$2a_3$	1.2 m
$2a_4$	1.4 m
b	3.0 m
b_5	1.0 m
b_6	0.4 m
c	2.0 m
c_1	0.6 m
G	180 kN
G_1	30 kN
G_2	20 kN

The parameters from TABLE 2 are inserted into formulas (13) to (25), and by solving these equations simultaneously, the analytical expression for the spatial force of the parallelogram support is derived.

$$P = \frac{1}{0.31+1.1\cos^2\gamma}\left(K_1 + K_2 \sin\gamma\cos\gamma\right) \tag{26}$$

$$P_E = \frac{1}{0.31\cos\gamma+1.1\cos^3\gamma}\left(K_3 + K_4 \sin\gamma\cos^2\gamma\right) \tag{27}$$

$$F_1 = \frac{1}{0.31+1.1\cos^2\gamma}(K_5 \cos^2\gamma + K_6 \sin\gamma\cos\gamma + K_7) \tag{28}$$

$$F_1' = \frac{1}{0.31+1.1\cos^2\gamma}(K_8 \cos^2\gamma + K_9 \sin\gamma\cos\gamma + K_{10}) \tag{29}$$

$$F_2' = \frac{1}{0.31+1.1\cos^2\gamma}(K_{14} \cos^2\gamma + K_{15} \sin\gamma\cos\gamma + K_{16}) \tag{30}$$

$$F_2' = \frac{1}{0.31+1.1\cos^2\gamma}(K_{14} \cos^2\gamma + K_{15} \sin\gamma\cos\gamma + K_{16}) \tag{31}$$

$$R_{1x} = \frac{1}{0.31\cos\gamma+1.1\cos^3\gamma}(K_{17} \cos^3\gamma + K_{18} \sin\gamma\cos^2\gamma + K_{19}) \tag{32}$$

$$R_{2x} = \frac{1}{0.31\cos\gamma + 1.1\cos^3\gamma}(K_{20}\cos^3\gamma + K_{21}\sin\gamma\cos^2\gamma + K_{22}) \tag{33}$$

$$R_{1y} = \frac{1}{0.31\sin\gamma + 1.1\cos^2\gamma\sin\gamma}(K_{23}\cos^3\gamma + K_{24}\sin\gamma\cos^2\gamma + K_{25}\cos\gamma + K_{26}\sin\gamma) \tag{34}$$

$$R_{2y} = \frac{1}{0.31\sin\gamma + 1.1\cos^2\gamma\sin\gamma}(K_{27}\cos^3\gamma + K_{28}\sin\gamma\cos^2\gamma + K_{29}\cos\gamma + K_{30}\sin\gamma) \tag{35}$$

$$R_{1z} = \frac{1}{0.31\cos\gamma + 1.1\cos^3\gamma}(K_{31}\cos^3\gamma + K_{32}\sin\gamma\cos^2\gamma + K_{33}) \tag{36}$$

$$R_{2z} = \frac{1}{0.31\cos\gamma + 1.1\cos^3\gamma}(K_{34}\cos^3\gamma + K_{35}\sin\gamma\cos^2\gamma + K_{36}) \tag{37}$$

In the formulas, (K_1) to (K_{36}) represent algebraic equations. The solution process is quite complex and is influenced by the length of the document, so it has been included in the attachment.

3.4. Stability analysis of multi-dimensional and multi-objective system of supports

3.4.1. Action type of roof

In steeply dipping coal seams with pseudo-inclined working faces, stress concentration occurs in the local roof of the working face, exerting additional load on the support. Simultaneously, the support generates a reverse load onto the roof. The impact of the roof on the support can be categorized into six types [24], illustrated in Fig. 5.

In the middle part of the working face, the roof's breaking form is complex. During the strike, the roof tilts backward, fractures, sinks, and rotates, exerting a squeezing and impact force on the support, thus facilitating the formation of squeezing and back-pushing on the support. The fractured upper part of the roof rotates around the contact point of the adjacent rock, serving as the axis of rotation, exerting pressure on the top beam. This often leads to the formation of tendencies for squeezing and anti-squeezing effects on the support. In the lower part, the gob is filled with gangue, resulting in a relatively stable roof structure that maintains full contact with the top beam, creating a positive effect.

Upon elucidating the specific type of interaction between the roof and the top beam and considering the practical engineering context of hydraulic support systems, the prevalent anti-tendency squeezing effect and frontal squeezing effect are identified to ascertain the direction of the roof load Q in the spatial mechanical model, depicted in Fig. 6.

With $\omega = \omega x = \omega y = 45°$ and $Q = 3200$ kN, the three constituent components of the roof load Q acting upon the top beam of the support are computed as follows: $Qz = 2263$ kN, oriented perpendicular to the top beam; $Qx = 1600$ kN, directed towards the coal wall; and $Qy = 1600$ kN, descending along the incline. Based on the support's movement trend, the friction force $f_x = \mu Q_z$

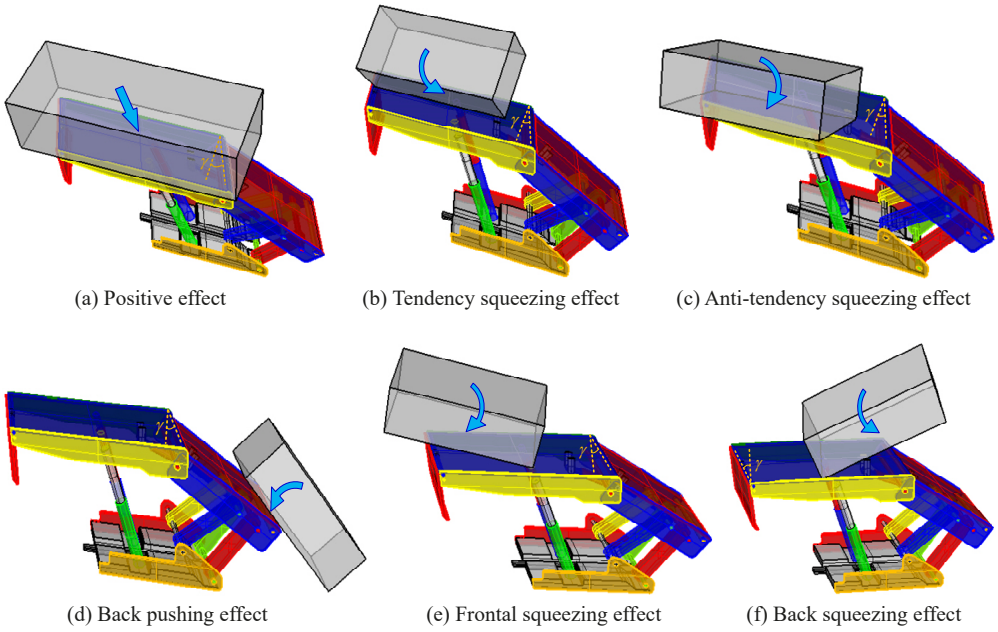

(a) Positive effect (b) Tendency squeezing effect (c) Anti-tendency squeezing effect

(d) Back pushing effect (e) Frontal squeezing effect (f) Back squeezing effect

Fig. 5. The action type of roof load

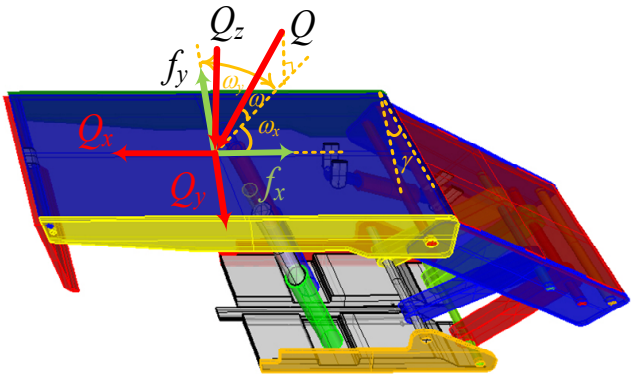

Fig. 6. Roof load direction in the spatial mechanical model

between the support and the roof is established, directed towards the goaf, while $f_y = \mu Q_z$ acts in an upward direction along the incline.

In the absence of considering the force exerted by the coal wall, the given parameters are substituted into equations (26) to (37). This process yields the correlation among the seam angle, pseudo-inclined angle, gangue force, roof load position, and the internal force of each support component. The results are shown in Figs. 7-10. The model's parameters are chosen based on the specific operational environment of the 3132 working face. The fundamental parameters are as follows: $Q_z = 2263$ kN, $Q_x = 1600$ kN, $Q_y = 1600$ kN, $f_x = f_y = \mu Q_z$, $\mu = 0.3$, $F_S = 50$ kN.

3.4.2. The influence of angle on the force evolution of support component

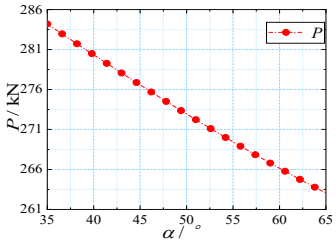

(a) The force evolution of column

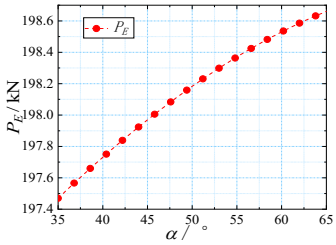

(b) The force evolution of balance jack

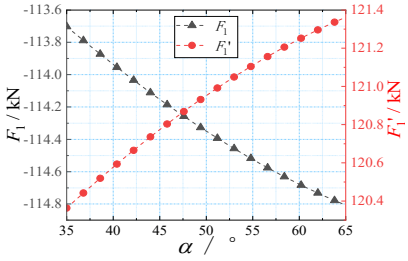

(c) The force evolution of front link

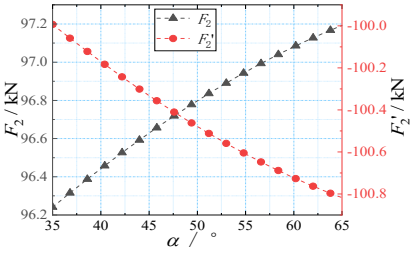

(d) The force evolution of back link

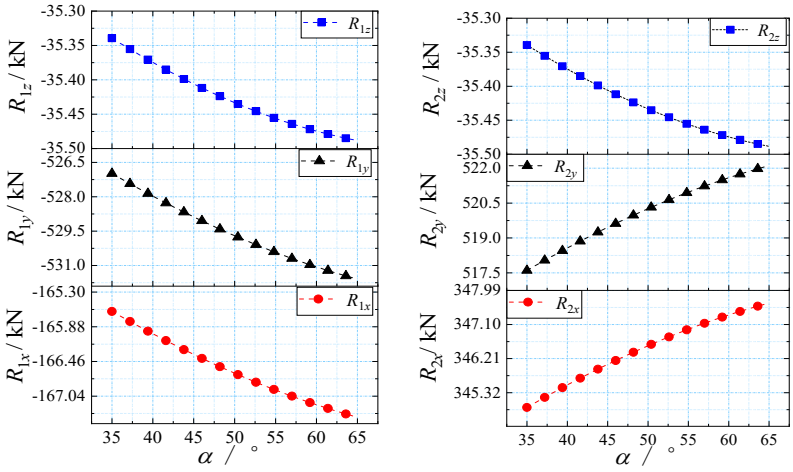

(e) The force evolution of hinge point between roof and shield beam

Fig. 7. The influence of angle on the force evolution of support component

As can be seen from Fig. 7:

(1) The working resistance P of the column diminishes gradually with the augmentation of the seam angle. As the seam angle increases, the working resistance PE of the balance jack elevates. The front link force F_1 experiences tension, while F_1' undergoes compression. The back link force F_2 encounters compression, whereas F_2' experiences tension.

Moreover, the constraint force at hinge point 1 of the top beam-shield beam and the constraint force component at hinge point 2 increase with the increasing seam angle.

(2) As the angle transitions from 35° to 65°, the working resistance P of the column diminishes from 508.3 kN to 506.3 kN. The working resistance PE of the balance jack escalates from 197.5 kN to 198.6 kN. The front connecting rod force F_1 surged from 113.7 kN to 114.8 kN, while F_1' escalated from 120.4 kN to 121.3 kN. The rear connecting rod force F_2 rose from 96.2 kN to 97.2 kN, and F_2' increased from 100.0 kN to 100.8 kN. The constraint force component R_{1z} of the top-shield beam hinge point 1 escalates from 35.33 kN to 35.50 kN, R_{1x} rises from 165.59 kN to 167.44 kN, and R_{1y} increases from 527.0 kN to 531.7 kN. The constraint force component R_{2z} of hinge point 2 escalates from 35.33 kN to 35.50 kN, R_{2x} rises from 345.76 kN to 347.52 kN, and R_{2y} increases from 517.5 kN to 521.2 kN. Overall, the working resistance of the column, the working resistance of the balance jack, the force of the front and back links, and the constraint force of the hinge point of the top-shield beam do not vary significantly with the angle of the seam.

(3) The primary role of the balance jack in the two-column shield hydraulic support is to modulate the angle of the top beam. This adjustment serves to regulate both the support force and the positioning of the resultant force, thereby enhancing the support system's adaptability to unstable roof conditions and maintaining it in an optimal operational state. In instances of significant roof fragmentation, the balance jack acts as a propulsive force, shifting the support force forward. This augmentation strengthens the support force at the front end of the top beam, preventing premature separation of the immediate roof and thereby preserving the roof's integrity. When the roof stability is relatively assured, the balance jack operates in tension mode to augment the roof-cutting capability at the rear end of the top beam. As the seam angle increases, the gravitational component force of the support along the incline also rises, exacerbating the risk of support toppling and sliding. When the support's top beam does not make full contact with the roof, it results in a reduction of the load borne by the top beam. The reduced contact between the top beam and the roof also decreases the force transmitted to the column, thereby lowering the working resistance of the column. To prevent support slippage, it's essential to increase the force exerted by the balance jack appropriately. Due to the angle, the vertical component of the constraint force at the hinge point of the top shield beam is minimal, with the tendency component outweighing both the trend and vertical components.

3.4.3. The influence of pseudo-inclined angle on the force evolution of support component

As can be seen from Fig. 8:

(1) The working resistance, denoted as P, of the column escalates in tandem with the rise of the pseudo-inclination angle. The working resistance, denoted as P_E, of the balance jack elevates proportionally with the escalation of the pseudo-inclination angle. The increase of the pseudo-inclined angle corresponds to a logarithmic escalation in F_1. Within the range of 33° to 45° for the pseudo-inclined angle, the growth trend of the curve is gradual. The relationship between F_1' and the pseudo-inclined angle follows a parabolic pattern. When the pseudo-inclined angle ranges from 0° to 20°, F_1' increases

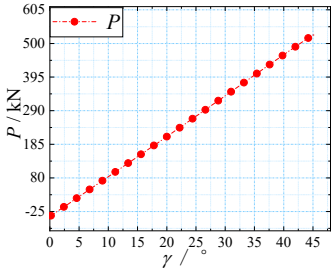

(a) The force evolution of column

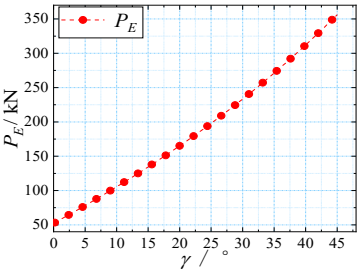

(b) The force evolution of balance jack

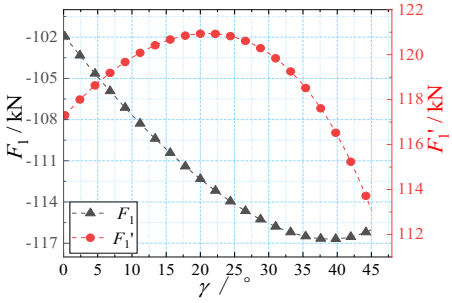

(c) The force evolution of front link

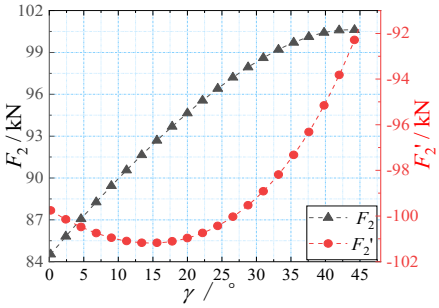

(d) The force evolution of back link

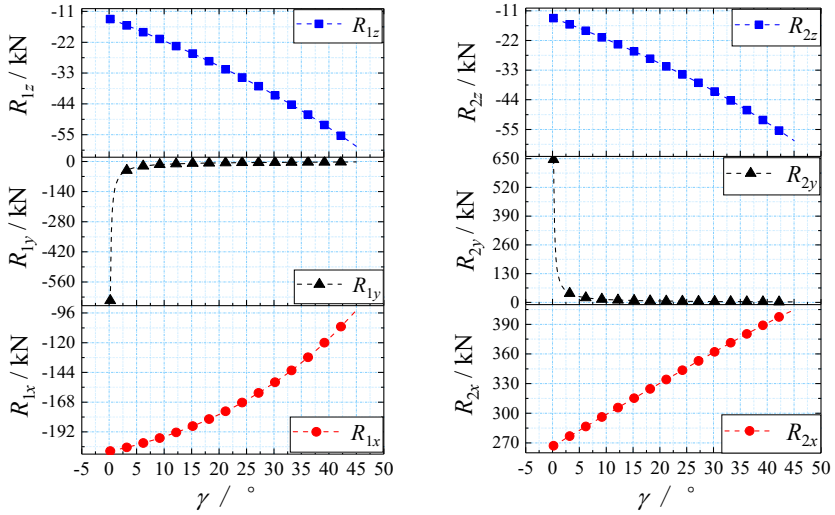

(e) The force evolution of hinge point between roof and shield beam

Fig. 8. The influence of pseudo-inclined angle on the force evolution of support component

with the angle's augmentation. When the pseudo-inclined angle ranges from 20° to 45°, it decreases with the increase of pseudo-inclined angle. The increase in F_2 corresponds to a logarithmic pattern with the augmentation of the pseudo-inclined angle. When the pseudo-inclined angle ranges from 38° to 45°, the curve's growth trend is gradual, and F_2

exhibits a parabolic relationship with the pseudo-inclined angle. When the pseudo-inclined angle falls within the range of 0° to 15°, it increases as the pseudo-inclined angle rises. Within the pseudo-inclined angle range of 15° to 45°, there is a decrease in the value as the pseudo-inclined angle increases. The constraint force R_{1z} at hinge point 1 of the top shield beam increases as the pseudo-inclined angle rises, while both R_{1x} and R_{1y} decrease with the augmentation of the pseudo-inclined angle. The constraint forces R_{2z} and R_{2x} at hinge point 2 increase as the pseudo-inclined angle increases, while R_{2y} decreases with the increase of the pseudo-inclined angle.

(2) As the pseudo-inclined angle varies from 0° to 45°, the working resistance \(P \) of the column escalates from –20 kN to 515 kN. The working resistance P_E of the balance jack rises from 50 kN to 350 kN. The front link force F_1 increases from 102 kN to 117 kN, while F_1' varies from 113 kN to 121 kN, reaching a maximum of 121 kN when the pseudo-inclined angle is 20°. The back link force F_2 increases from 84 kN to 101 kN, while F_2' varies from 92 kN to 101 kN. When the pseudo-inclined angle is 15°, it reaches the maximum value of 101 kN. The constraint force component R_{1z} of the top beam-shield beam hinge point 1 increases from 11 kN to 55 kN, R_{1x} decreases from 216 kN to 108 kN, and R_{1y} decreases from 646 kN to 2.4 kN. The constraint force component R_{2z} of hinge point 2 increases from 11 kN to 55 kN, R_{2x} increases from 270 kN to 405 kN, and R_{2y} decreases from 646 kN to 2.3 kN. Overall, the working resistance of the column, the working resistance of the balance jack, the force of the front and back links, and the constraint force of the hinge point of the top-shield beam are significantly influenced by the pseudo-inclined angle.

(3) When the seam angle remains constant, the angle of the working face decreases as the pseudo-oblique angle increases, leading to a continuous decrease in the area of the hollow face in the gob behind the support. During the caving and filling process, the gangue's impact and contact effects on the tail of the support become more pronounced and intense, leading to an increase in the support's bearing capacity. To ensure the stability of the support system, the working resistance of both the column and the balance jack is increased. The alignment of the top beam of the parallelogram support with the angle between the coal seam and the strike of the working face necessitates adjustments in response to changes in the pseudo-inclined angle. As the pseudo-inclined angle increases, it results in a larger exposed area of the tail beam of the support along the strike. The force components at the hinge point of the top shield beam, including both the inclined and strike components, undergo significant changes due to the influence of falling gangue in the goaf.

3.4.4. The influence of gangue on the force evolution of support component

As can be seen from Fig. 9:

(1) The working resistance P of the column progressively rises with the escalation of gangue force. As the gangue force increases, the working resistance P_E of the balance jack experiences changes: the front link force F_1 shifts towards tension, while F_1' transitions to pressure. Similarly, the back link force F_2 becomes pressure-oriented, while F_2' turns into tension. Additionally, the constraint force at hinge point 1 of the top-shield beam and its associated component at hinge point 2 diminishes.

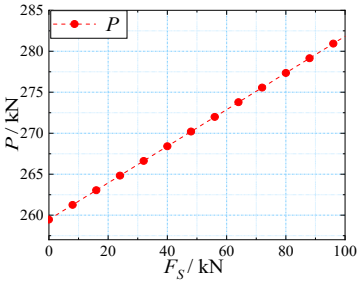

(a) The force evolution of column

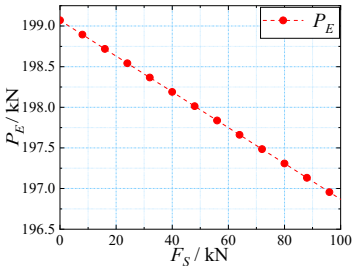

(b) The force evolution of balance jack

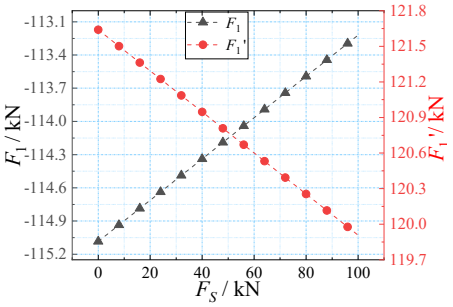

(c) The force evolution of front link

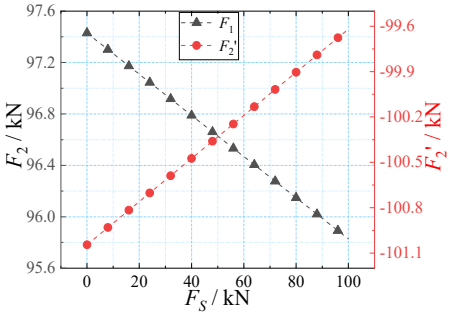

(d) The force evolution of back link

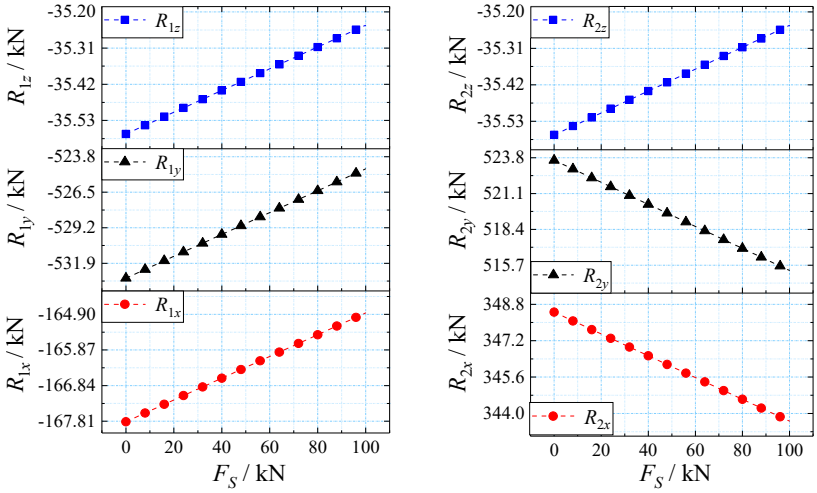

(e) The force evolution of hinge point between roof and shield beam

Fig. 9. The influence of gangue on the force evolution of support component

(2) As the gangue force F_S varies from 0 to 100 kN, the working resistance P of the column rises from 260 kN to 282 kN. The working resistance P_E of the balance jack decreases from 199.2 kN to 196.8 kN. F_1 decreases from 115.1 kN to 113.2 kN, and F_1' decreases from 121.7 kN to 119.8 kN. Meanwhile, F_2 decreases from 97.4 kN to 95.8 kN, and F_2'

decreases from 101.1 kN to 99.6 kN. R_{1z} decreases from 35.58 kN to 35.25 kN, R_{1x} decreases from 167.81 kN to 164.90 kN, and R_{1y} decreases from 533.3 kN to 525.1 kN. Similarly, R_{2z} decreases from 35.58 kN to 35.25 kN, R_{2x} decreases from 348.6 kN to 343.4 kN, and R_{2y} decreases from 523.8 kN to 515.7 kN. Indeed, the gangue force exerts influence across various aspects, including the working resistance of the column, the balance jack, the front and back link forces, and the constraint force at the hinge point of the top-shield beam. Among these, its impact on the working resistance of the column appears to be the most significant.

(3) In the pseudo-inclined working face, the support is subject to loading conditions that reflect the regional characteristics of the mine environment. The gangue force F_S demonstrates a pronounced effect on the support in the middle and lower regions of the working face, while its impact is comparatively weaker on the support in the upper portion. The variation in gangue force F_S from small to large can be interpreted as the impact of gangue on the support throughout the upper, middle, and lower sections of the working face. When the seam angle and pseudo-oblique angle remain constant, the working resistance of the support in the middle and lower sections of the working face exceeds that in the upper portion to counteract the influence of gangue.

3.4.5. The influence of position of roof load on the force evolution of support component

As can be seen from Fig. 10:

(1) The working resistance P of the column tends to gradually increase with the rise in the roof load position. The working resistance P_E of the balance jack, the tension in the front link force F_1, the pressure in F_1', the pressure in the back link force F_2, the tension in F_2', and the constraint force at hinge point 1 of the top-shield beam, as well as the constraint force component at hinge point 2, all decrease with the elevation of the roof load position.

(2) As the position of the roof load a_2 varies from –0.75 m to 0.75 m, the working resistance P of the column increases from –400 kN to 1000 kN. The working resistance P_E of the balance jack decreases from 310 kN to 85 kN. F_1 decreases from 180 kN to 50 kN, and F_1' decreases from 180 kN to 60 kN. F_2 decreases from 150 kN to 58 kN, and F_2' decreases from 149 kN to 52 kN. R_{1z} at the hinge point 1 of the top-shield beam decreases from 40.8 kN to 29.4 kN, R_{1x} decreases from 284 kN to 68 kN, and R_{1y} decreases from 908 kN to 214 kN. R_{2z} at hinge point 2 decreases from 69 kN to 1.8 kN, R_{2x} decreases from 560 kN to 140 kN, and R_{2y} decreases from 897 kN to 208 kN. Indeed, the overall working resistance of the column, the working resistance of the balance jack, the forces in the front and back links, and the constraint forces at the hinge points of the top-shield beam exhibit significant changes with variations in the position of the roof load. These changes reflect the dynamic nature of the structural response under varying loads.

(3) The fundamental consequence of altering the position of the roof load lies in the resultant movement and deformation failure of the roof structure. As the movement state of the roof shifts, it induces variations in the interaction between the support structure and the surrounding rock formation, thereby manifesting as fluctuations in the passive load exerted on the support system. When the roof load is applied at the edge of the top beam of the support, significant force is exerted on the front and back links and the hinge point of the top shield beam on the same side. This notably affects the working resistance

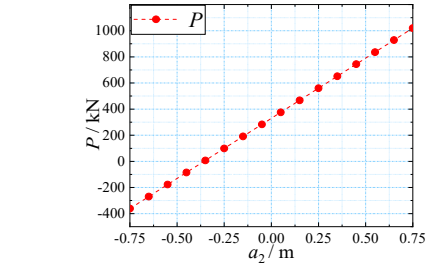

(a) The force evolution of column

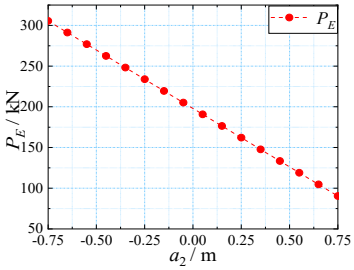

(b) The force evolution of balance jack

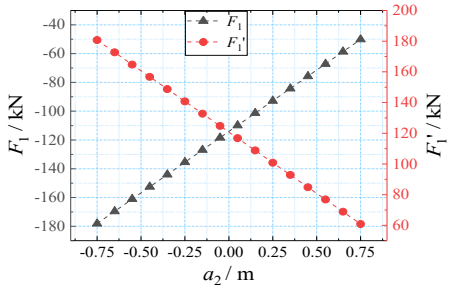

(c) The force evolution of front link

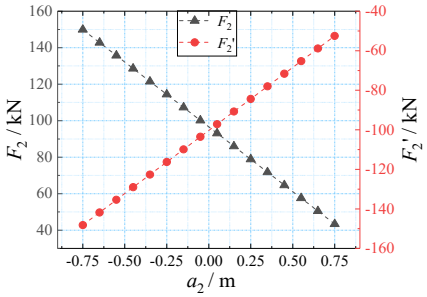

(d) The force evolution of back link

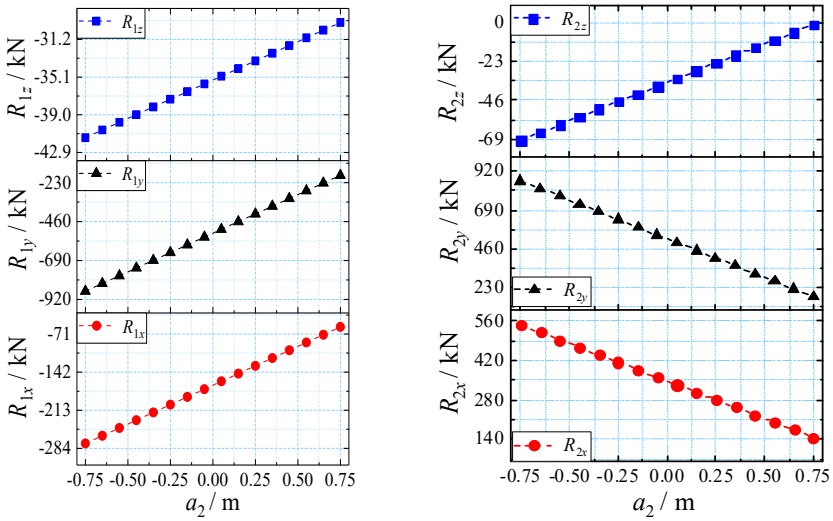

(e) The force evolution of hinge point between roof and shield beam

Fig. 10. The influence of position of roof load on the force evolution of support component

of the column, with the maximum value reaching 1000 kN, making the column prone to deformation and failure. Additionally, the top beam of the support is affected by the eccentric load, which compromises the stability of the support, increasing the risk of tipping and sliding.

4. Numerical analysis of stress and deformation characteristics of support

4.1. Establishment of the model

Using Rhino software, three-dimensional models of rectangular and parallelogram hydraulic supports were created, with the ZYJ3200/14/32 fully mechanized mining hydraulic support as the reference object. Each group contained seven equally spaced supports, numbered sequentially from bottom to top as 1-7# supports. The support model has a maximum height of 3.2 meters, a width of 1.5 meters, and a maximum working resistance of 3200 kilonewtons. The support structure primarily comprises a top beam, shield beam, column, front link, back link, base, and balance jack. Additionally, pivotal points include those of the front link, back link, shield-top beam, balance jack, and column hydraulic jack. The three-dimensional model of the support is depicted in Fig. 11.

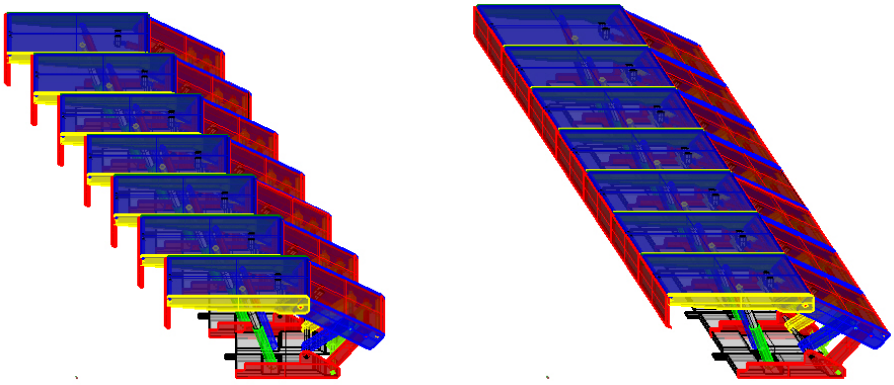

(a) Rectangular support model (b) Parallelogram support model

Fig. 11. Spatial model of support

After importing and simplifying the model, the mesh of the model is segmented using the ANSYS Workbench module. The ANSYS software encompasses numerous computational units, facilitating the analysis of a wide array of practical problems with ease. Typically, there are three types of elements in ANSYS: plane stress, shell, and solid elements. Under normal circumstances, the appropriate unit type is chosen based on the complexity of the engineering structure. In this study, the meshing of the two-column shield hydraulic support is conducted using solid elements. The base mesh size for the model ranges from 5 to 8 mm. The model primarily consists of quadrilateral shell 181 elements, with triangular elements used for transitions, and solid 185 elements that are predominantly hexahedral. In total, the model contains 150,404 elements.

To simulate the support's performance more accurately, revolute joints are employed to replicate the rotational relationships of the top-shield beam hinge, shield beam-front and back link hinges, and front and back link-base hinges. The material for each structural component of the support is steel, with an elastic modulus of 205 GPa, a Poisson's ratio of 0.3, and a density of

7.8×10^{-9} t/mm^3. The base is constrained, a fixed support is placed on the side of the 1# bracket, and a contact relationship is defined for the side guard plate between the brackets.

4.2. External load setting

4.2.1. Regional load characteristics of supports

The 3132 working face is equipped with 67 ZZ6500/22/48 shield hydraulic supports and 3 ZZG6500/22/48 transitional supports. The dynamic mining pressure detector is employed to monitor the mining pressure of the working face. Specifically, the 16# support (lower area), the 32# support (middle area), and the 48# support (upper area) are monitored, and the data are then statistically processed. The results are presented in TABLE 3.

TABLE 3

Working resistance of support in different areas of 3132 working face

Measurement area / support	The interval of working resistance / MPa	The frequency of working resistance / %	Average of support resistance / MPa
Lower area 16# support	<6	2.86	24.5
	6~12	4.14	
	12~18	5.42	
	18~24	38.15	
	24~30	47.41	
	30~36	2.02	
Middle area 32# support	<6	0	28.88
	6~12	5.00	
	12~18	6.25	
	18~24	21.88	
	24~30	31.25	
	30~37	35.62	
Upper area 48# support	<6	0	27.17
	6~12	7.50	
	12~18	13.13	
	18~24	34.38	
	24~30	25.00	
	30~35	20.00	

The field observation findings from the 3132 working face in Lvshuidong Mine indicate that the load distribution of the support in the pseudo-inclined working face within steeply dipping coal seams exhibits distinct regional characteristics. The load on the support in the middle area of the working face is the greatest, followed by the upper area and then the lower area. The maximum load on the 16# support in the lower part is 31 MPa, with an average of 24.5 MPa. For the 32# support in the middle part, the maximum load is 37 MPa, with an average of 28.88 MPa. Lastly, the maximum load on the 48# support in the upper part is 35 MPa, with an average of 27.17 MPa. The load variation of the support in the middle and upper areas is significant, indicating severe roof breaking in the working face. Periodic weighting is evident, and there is

susceptibility to the impact of caving gangue. The load variation in the lower area is minimal, indicating a relatively stable “support-surrounding rock” system, and the working resistance of the support remains stable.

4.2.2. External load setting

Based on the regional load characteristics of the support, the seven support models are divided into three areas to simulate the supports in the upper, middle, and lower areas of the working face. Based on the statistical data from the mine pressure monitoring in TABLE 3, a variable load perpendicular to the top beam in one direction is applied to the top beam of the three regional supports to equalize the roof load.

For the 6# and 7# supports, which are the upper supports of the working face, the variable load ranges from a minimum of 980 kN to a maximum of 3400 kN, with a stable load of 2600 kN. The 3-5# support serves as the middle support of the working face. The variable load ranges from a minimum of 590 kN to a maximum of 3600 kN, with a stable load of 2800 kN. The 1#

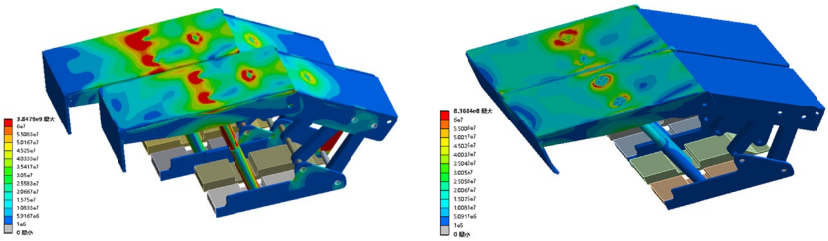

(a) Supports in the upper area

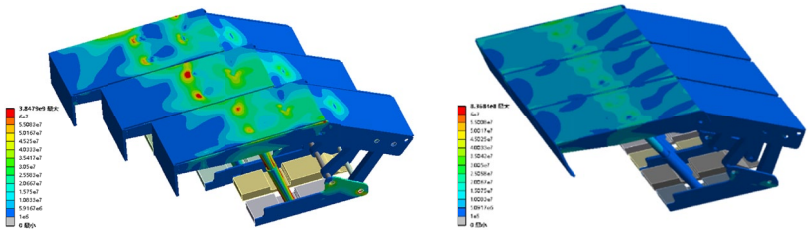

(b) Supports in the middle area

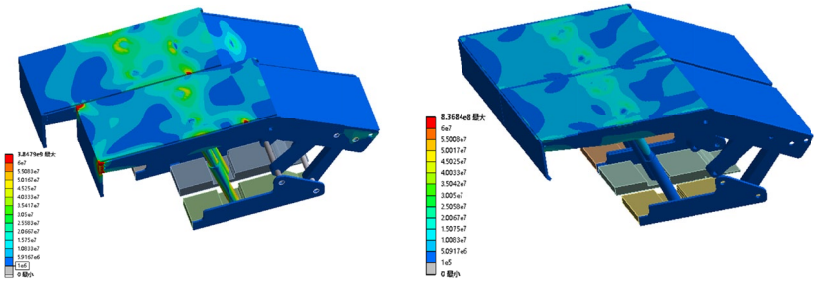

(c) Supports in the lower area

Fig. 12. Comparison of support stress distribution under minimum load

and 2# supports are the lower supports of the working face. For the 1# and 2# supports, the minimum value of the variable load is 300 kN, the maximum value is 3100 kN, and the stable load is 2400 kN. At the same time, a inter-frame force of 120 kN is applied on the side of the 7# support, while a force ranging from 0 to 100 kN is applied on the side of the back link of the supports (1-5#) in the middle and lower part of the working face.

4.3. Comparison of stress evolution of support

From Fig. 12-14, it's evident that the stress distribution of the support exhibits clear regional characteristics. When the roof load is small, the stress on the support in the upper part of the working face is indeed the greatest. This is because the upper supports bear more weight from the overlying strata, especially when the roof load is reduced. As the roof load increases and stabilizes, the stress on the supports in the middle area of the working face gradually increases. This is due to the redistribution of the load as the roof load becomes more uniform, causing the middle supports to bear a larger portion of the weight. The presence of more stress concentration

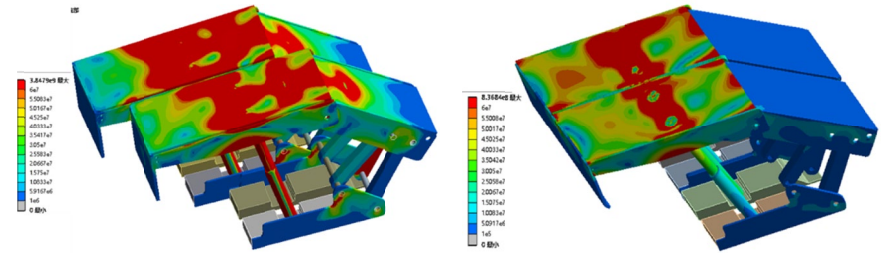

(a) Supports in the upper area

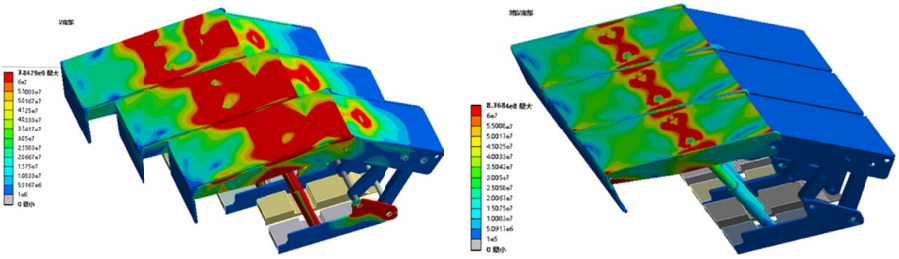

(b) Supports in the middle area

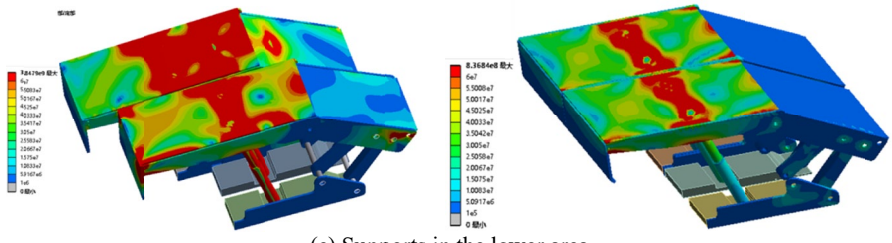

(c) Supports in the lower area

Fig. 13. Comparison of support stress distribution under maximum load

areas in the middle and upper areas of the working face suggests that the roof in these areas is relatively more active, indicating movements or settlements that result in increased load on the supports there. This could be due to geological factors, variations in mining conditions, or other dynamic changes in the roof strata that make these regions particularly sensitive to changes in roof load. The maximum stress of the rectangular support is primarily concentrated at the following areas: the connection between the column and the top beam, the back end of the top beam, and the connection points between the balance jack and the top beam, as well as the shield beam. These are the critical points where the support structure experiences the highest levels of force and strain. For the parallelogram bracket, similar to the rectangular support, the maximum stress is typically found at the connection between the column and the top beam. In contrast, the stress on the shield beam is relatively small compared to other parts of the support structure. This highlights the structural design and load-bearing characteristics specific to the parallelogram bracket configuration. Comparatively, the rectangular bracket demonstrates a broader stress distribution exceeding 60 MPa, with pronounced loading observed on both the top beam and the shield beam, contrasting with the parallelogram bracket configuration.

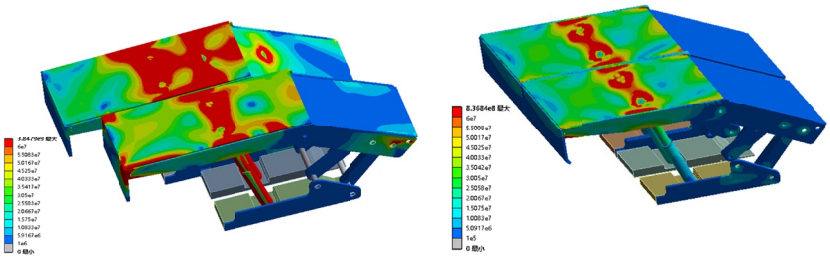

(a) Supports in the upper area

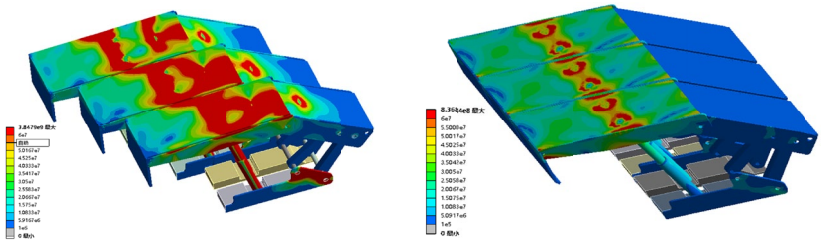

(b) Supports in the middle area

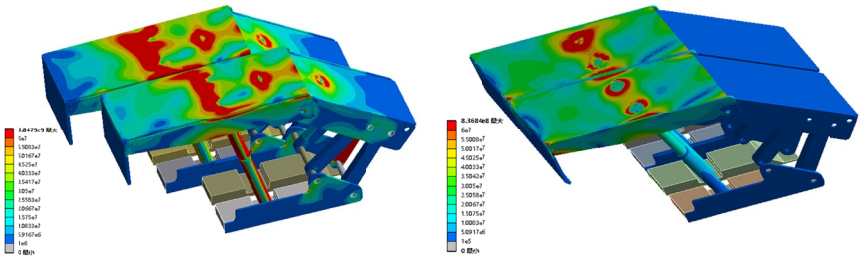

(c) Supports in the lower area

Fig. 14. Comparison of support stress distribution under stable load

4.4. Comparison of deformation evolution of support

The support deformation exhibits distinct regional characteristics, as depicted in Figs. 15-17. When subjected to a minor roof load, the upper portion experiences the most significant support deformation. As the roof load intensifies and reaches a steady state, the support deformation becomes most pronounced in the middle and upper sections. This observation indicates that during the mining operation, the gob in the lower section of the working face becomes filled with gangue, providing effective support for the roof and resulting in relatively stable support conditions. The roof in the middle and upper sections of the working face exhibits greater activity, leading to increased susceptibility to support instability. The maximum overall deformation of the rectangular support measures 0.18 meters, primarily concentrated at the front end of the top beam, with secondary deformation observed at the hinge joint between the top and shield beams. The overall maximum deformation of the parallelogram support is 0.01 meters, likewise concentrated primarily at the front end of the top beam. Compared to the rectangular support, the

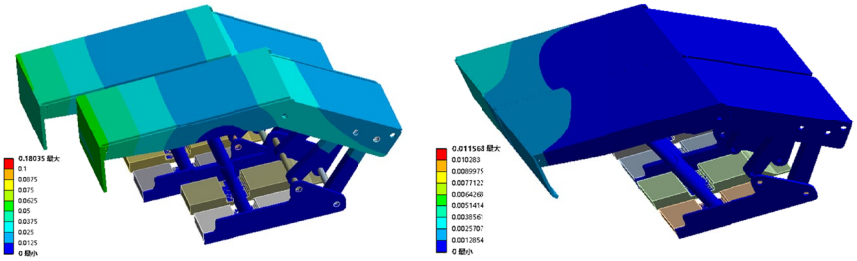

(a) Supports in the upper area

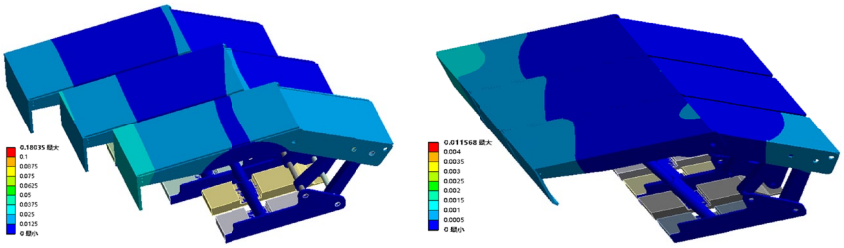

(b) Supports in the middle area

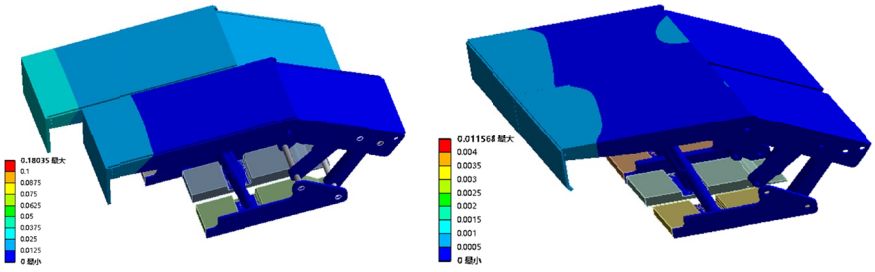

(c) Supports in the lower area

Fig. 15. Comparison of support deformation distribution under minimum load

parallelogram support exhibits lesser overall deformation, with notably reduced deformation at the connections between the column, top beam, and shield beam. This observation suggests that the parallelogram support possesses superior load-bearing capacity and stability.

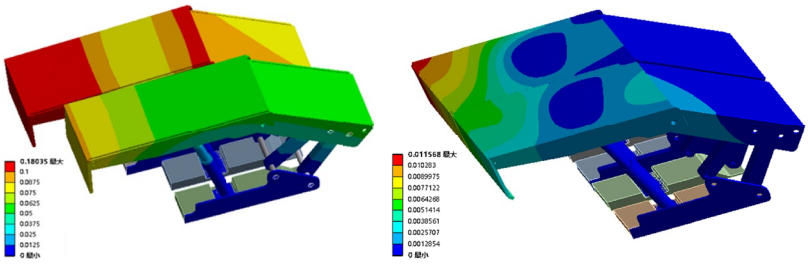

(a) Supports in the upper area

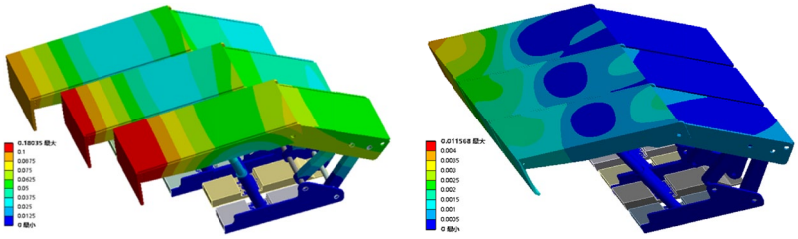

(b) Supports in the middle area

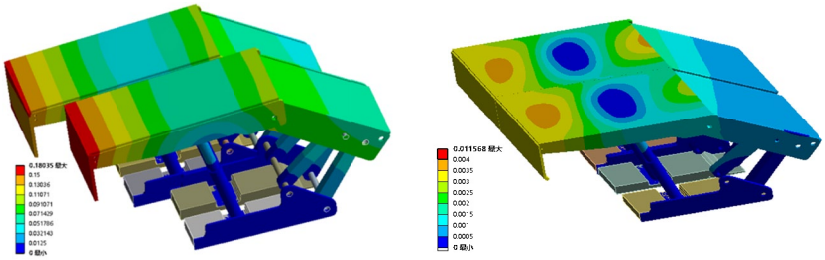

(c) Supports in the lower area

Fig. 16. Comparison of support deformation distribution under maximum load

5. Discussions

Based on the findings outlined above, a hydraulic support control technology is proposed for pseudo-inclined working faces, aimed at achieving safe and efficient mining operations.

(1) Anti-sliding technology of hydraulic support:

The implementation of an active anti-falling and anti-skid mechanism involves utilizing guard plates situated within the top beam and adjusting beams of the base. Through the manipulation of jacks, these components facilitate the controlled movement of adjacent supports, effectively mitigating the occurrence of falling and sliding during support relocation. Strive to ensure that

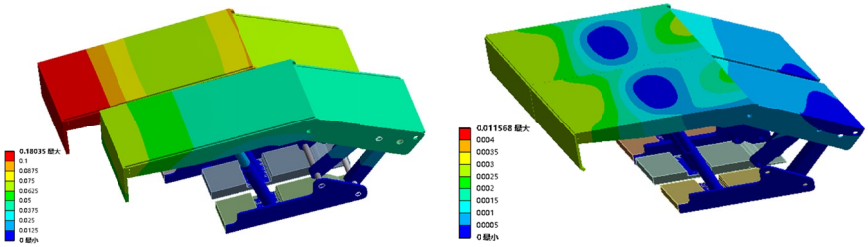

(a) Supports in the upper area

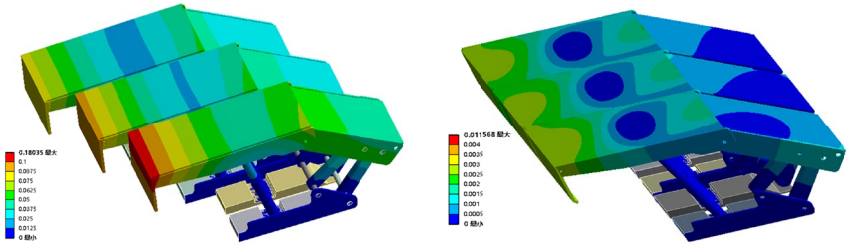

(b) Supports in the middle area

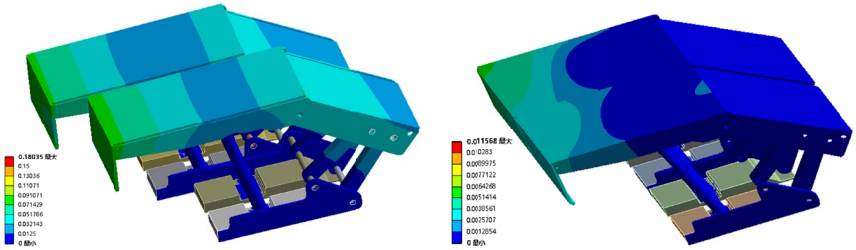

(c) Supports in the lower area

Fig. 17. Comparison of support deformation distribution under stable load

the hydraulic support guard plate remains parallel to the conveyor. The terminal support plays a pivotal role in preventing support collapse and skidding within the mining face. Two hydraulic jacks are installed beneath the top beam between every two hydraulic supports (one preceding and one following each), with an additional two jacks positioned on the base (one preceding and one following each) for every 3 to 5 hydraulic supports at the lower end. Any minor slipping occurrences during the hydraulic support pushing process can be rectified using the jack adjusting device, ensuring proper support alignment to uphold both the roof and floor. The inclusion of a spring (φ16 steel wire) between the top beam and the shield beam serves as an additional safety measure. In situations where the jack pushing action by the support proves ineffective, the spring functions to provide an anti-falling effect.

(2) Electro-hydraulic control technology:

Electro-hydraulic control technology is employed to achieve comprehensive and integrated control of the hydraulic support system. Using the single support of the working face as the baseline, an adjacent support structure is selected and configured as a unified support group. Upon

receiving the command, both the single action and complex action modes of the hydraulic support initiate operation. Within the same support group, supports automatically move in a sequential or interval-based manner based on predefined rules. In the process of advancing the conveyor, it's common for five hydraulic supports to operate in tandem. This coordinated effort helps ensure stability and support along the conveyor route. The electro-hydraulic control parameters are accessible and can be displayed on a remote display platform for monitoring and adjustment purposes. The control terminal provides visibility into various parameters, including the upper and lower limit thresholds, the rehydration time, the interval between rehydration, and the total number of rehydration cycles. This information allows for precise monitoring and management of the hydraulic support system. Once the pressure reaches a predetermined threshold, the integrated system autonomously executes the lifting column command and restores the pressure to the specified normal value. This feature ensures the hydraulic support system maintains optimal functionality without requiring manual intervention. In response to the conditions within the mine, the ability to set and adjust data online proves crucial for optimizing the strength and efficiency of hydraulic support systems.

6. Conclusions

(1) The working resistance of the column decreases gradually as the angle of the seam increases. As the angle increases, the working resistance of the balance jack, the front link force, the back link force, and the force exerted on hinge points 1 and 2 all experience an increase. As the angle increases, the gravitational component acting on the support along the incline also increases, exacerbating the risk of support falling and sliding. The reduced contact between the top beam of the support and the roof leads to a decrease in the working resistance of the column. To enhance the support's ability to uphold the roof and prevent slippage, it's advisable to appropriately increase the thrust exerted by the balance jack.

(2) When the seam angle remains constant, the working face angle decreases as the pseudo-inclination angle increases, resulting in an increase in both the working resistance of the column and the working resistance of the balance jack. This phenomenon indicates a correlation between the pseudo-inclination angle and the load-bearing requirements of the support system, suggesting a need for careful adjustment and monitoring to maintain stability and safety in mining operations. The constraint force at the hinge point experiences significant changes in both its inclined and strike components. When the angle and pseudo-inclination angle of the coal seam remain constant, the working resistance of the support in the middle and lower parts of the working face exceeds that of the support in the upper part, primarily to counteract the influence of gangue. When the roof load is applied to the edge of the top beam of the support, it exerts greater force on the front and rear links, as well as on the hinge points of the top beam-shield beam on the same side. This results in the most noticeable change in the working resistance of the column. This phenomenon highlights the importance of ensuring adequate support and reinforcement in response to varying loads to maintain the stability and safety of the mining operation.

(3) Support stress distribution exhibits distinctive regional characteristics. In the middle and upper sections of the working face, numerous stress concentration zones are observed.

The roof in the middle and upper regions of the working face demonstrates comparatively heightened activity, necessitating notable support loading. The primary concentration of maximum stress in the rectangular support occurs at the junctions between the column and top beam, the rear end of the top beam, as well as the connections linking the balance jack, top beam, and shield beam. Maximum stress in the parallelogram support is primarily observed at the junction between the column and the top beam, with relatively minor stress on the shield beam. In comparison to the parallelogram support, the rectangular support exhibits a broader stress distribution exceeding 60 MPa, particularly evident in the increased loading of the top beam and shield beam.

(4) The regional characteristics of support deformation are readily discernible. When subjected to minimal roof loading, the most pronounced support deformation occurs in the upper section of the working face. As the roof load intensifies and approaches stability, the most significant support deformation is observed in the middle and upper sections of the working face. The maximum overall deformation of the rectangular support reaches 0.18 m, primarily concentrated at the front end of the top beam, followed by the hinge joint between the shield beam and the top beam. The total maximum deformation of the parallelogram support measures 0.01 m, predominantly concentrated at the front end of the top beam. Relative to the rectangular support, the parallelogram support exhibits minimal overall deformation, particularly notable is the reduced deformation at the junctions between the column and the top beam, as well as the shield beam, in comparison to the rectangular support.

Date Availability

The data used to support the findings of this study are available from the corresponding author upon request.

Conflicts of Interest

This manuscript has not been published or presented elsewhere in part or in entirety and is not under consideration by another journal. We have read and understood your journal's policies, and we believe that neither the manuscript nor the study violates any of these. There are no conflicts of interest to declare.

Acknowledgment

This work was supported by the National Natural Science Foundation of the PRC (52274139), National Key R & D Program Funded Project (2023YFC2907502) and the 76nd batch of General Project Funded by China Postdoctoral Science Foundation (2024M760017).

References

[1] Y.P. Wu, D.F Yun, P.S. Xie, et al., Progress, practice and scientific issues in steeply dipping coal seams fully-mechanized mining [J]. Journal of China Coal Society **45** (01), 24-34 (2020). (in Chinese)

[2] J.A. Wang, J.L. Jiao, Criteria of support stability in mining of steeply inclined thick coal seam [J]. International Journal of Rock Mechanics and Mining Sciences **82** (02), 22-35 (2016).

[3] Y.P . Wu, P.S. Xie, D.F. Yun, et al., Theory and practice of fully mechanized longwall mining in steeply dipping coal seams [J]. Mining Engineering **65** (01), 35-41 (2013).

[4] G.F. Wang, Y.J. Xu, D.Y. Li, Analysis on supporting principle and its application of powered support in large inclined fully mechanized face based on balance of rigid and flexible combined overturning moment [J]. Chinese Journal of Rock Mechanics and Engineering **37** (S2), 4125-4132 (2018). (in Chinese)

[5] P.S. Xie, Y.Y. Zhang, Y.L. Zhang, et al., Instability law of the coal-rock interbedded roof and its influence on supports in large mining height working face with steeply dipping coal seam [J]. Journal of China Coal Society **46** (02), 344-356 (2021).

[6] S.H. Luo, T. Wang, Y.P. Wu, et al., Internal mechanism of asymmetric deformation and failure characteristics of the roof for longwall mining of a steeply dipping coal seam [J]. Archives of Mining Sciences **66** (01), 101-124 (2021).

[7] H. Zhang, Y.P. Wu, P.S. Xie, Coal wall instability evolution law of large mining height face in steeply dipping hard roof soft coal seam [J]. Mathematical Problems in Engineering (2022). DOI: https://doi.org/10.1155/2022/9683067

[8] X. Liu, Mechanism and control technology of support instability in fully-mechanized mining face in thick coal seam with large dip angle and fault [J]. Coal Science and Technology **49** (10), 16-22 (2021). (in Chinese)

[9] B.S. Hu, Y.P. Wu, H.W. Wang, et al., Risk mitigation for rockfall hazards in steeply dipping coal seam: a case study in Xinjiang, northwestern China [J]. Geomatics, Natural Hazards and Risk **12**, 1, 998-1014 (2020).

[10] Y.P. Wu, B.S. Hu, D. Lang, et al., Risk assessment approach for rockfall hazards in steeply dipping coal seams [J]. International Journal of Rock Mechanics and Mining Sciences **138**, 104626 (2021).

[11] J.C. Wang, W.J. Wei, J.W. Zhang, Stability analysis of support around the longwall top-coal caving mining in steeply thick coal seam [J]. Journal of China Coal Society **42** (11), 2783-2791 (2017). (in Chinese)

[12] Y. Yuan, S.H. Tu, F.J. Dou, et al., Support instability mechanism of fully mechanized top coal caving face with steep coal seams and its control [J]. Journal of Mining & Safety Engineering **25** (04), 430-434 (2008).

[13] S.H Luo, T. Wang, Y.P. Wu, et al., Stability analysis of "support-surrounding rock" system for fully mechanized longwall mining in steeply dipping coal seams [J]. Shock and Vibration (2022).
DOI: https://doi.org/10.1155/2022/5376718

[14] X.L Chi, K. Yang, Q. Fu, Analysis of regenerated roof and instability support control countermeasures in a steeply dipping working face [J]. Energy Exploration & Exploitation **38** (4), 1082-1098 (2019).

[15] Y.P. Wu, B.S. Hu, P.S. Xie, A new experimental system for quantifying the multidimensional loads on an on-site hydraulic support in steeply dipping seam mining [J]. Experimental Techniques **43** (05), 571-585 (2019).

[16] C. Ross, D. Conover, J. Baine, Highwall mining of thick, steeply dipping coal-a case study in geotechnical design and recovery optimization [J]. International Journal of Mining Sciences and Technology **29** (5), 777-780 (2019).

[17] D.F. Yun, Z. Liu, W.D. Cheng, et al., Monitoring strata behavior due to multi-slicing top coal caving longwall mining in steeply dipping extra thick coal seam [J]. International Journal of Mining Sciences and Technology **27** (S1), 179-184 (2017).

[18] Y.P. Wu., Controlling pattern for dynamic stability of system "roof-support-floor" [J]. Journal of China Coal Society **32** (4), 341-346 (2007). (in Chinese)

[19] X.L. Chi, K. Yang, Q. Fu, et al., The mechanism of mining-induced stress evolution and ground pressure control at irregular working face in inclined seams [J]. Geotechnical and Geological Engineering **38**, 91-107 (2020).

[20] Q.J. Zhan, N. M. Shahani, Z.C. Xue, et al., Law of coal caving behind the flexible shield support in pseudo-inclined working face [J]. Plos One **16** (12), e0261355 (2022).

[21] P.S. Xie, Y.Y. Zhang, Y.P. Wu, et al., Experimental study on roof fracture and gangue filling in pitching oblique mining area of steeply dipping medium thick coal seam [J]. Journal of Mining & safety Engineering **40** (3), 534-542 (2023). (in Chinese)

[22] Y.P. Wu, Y.B. Yang, T. Wang, et al., Stability analysis of support under gangue filling condition in pitching oblique mining area of steeply dipping seam [J]. Coal Science and Technology **50** (1), 60-69 (2022).

[23] G.F. Wang, Hydraulic Support Technology [M]. Beijing: China Coal Industry Publishing House (1999). (in Chinese)

[24] P.S. Xie, Response of overburden structure and its stability around the longwall mining face area in steeply dipping seam [D]. Xi'an: Xi'an University of Science and Technology (2011). (in Chinese)